A viable method to predict acoustic streaming in presence of cavitation

Olivier Louisnard

A viable method to predict acoustic streaming in presence of cavitation

O. Louisnard

Centre RAPSODEE, UMR CNRS 5302, Université de Toulouse, Ecole des Mines d'Albi, 81013 Albi Cedex 09, France

Keywords:
Acoustic cavitation
Acoustic streaming
Propagation in bubbly liquids
Bjerknes force

A B S T R A C T

The steady liquid flow observed under ultrasonic emitters generating acoustic cavitation can be successfully predicted by a standard turbulent flow calculation. The flow is driven by the classical averaged volumetric force density calculated from the acoustic field, but the inertial term in Navier–Stokes equations must be kept, and a turbulent solution must be sought. The acoustic field must be computed with a realistic model, properly accounting for dissipation by the cavitation bubbles [Louisnard, Ultrason. Sonochem., 19, (2012) 56-65]. Comparison with 20 kHz experiments, involving the combination of acoustic streaming and a perpendicular forced flow in a duct, shows reasonably good agreement. Moreover, the persistence of the cavitation effects on the wall facing the emitter, in spite of the deflection of the streaming jet, is correctly reproduced by the model. It is also shown that predictions based either on linear acoustics with the correct turbulent solution, or with Louisnard's model with Eckart–Nyborg's theory yields unrealistic results.

1. Introduction

The propagation of acoustic waves (and of ultrasound in particular) in fluids is accompanied by steady flows, known as "acoustic streaming" [1–6]. The latter expression covers in fact various mechanisms, which can be divided into two main families, possibly occurring together: streaming near a solid boundary and streaming in unbounded fluid. The latter mechanism can be observed systematically in acoustic cavitation experiments, where a noticeable jet-like flow appears, as if it were expelled from the transducer.

The velocity fields of such flows have been evaluated either by visual observation [7], laser Doppler anemometry (LDA) [8,9], or particle image velocimetry (PIV) [10–13]. Using the latter method, Mettin and co-workers showed that the appearance of cavitation increased 30-fold the streaming velocities [14]. The corresponding flow was found to be turbulent, in agreement with the corresponding Reynolds number. Dubus and co-workers [15] mentioned that acoustic streaming currents generally hides the conical structure [16–18] visible under sonotrodes. They managed to suppress streaming by using pulsed ultrasound. Hihn and co-workers explored the combination of upward acoustic streaming above a transducer with a forced transverse horizontal flow in a rectangular duct [19,20]. They measured the deflection of the streaming jet by PIV as the velocity of the forced transverse flow was increased. Strangely enough, the authors found that even when the streaming jet was strongly deflected by the forced flow, cavitation remained active on the wall opposed to the transducer.

So far, no theory of acoustic streaming in presence of cavitation has been developed. In particular, there is no theoretical result available to quantitatively predict the velocities observed and explain why they are much larger in presence of cavitation.

The aim of this paper is to propose such a model, or rather an add-on to the model of wave propagation accounting for cavitation presented in Ref. [21]. The latter was found to predict correctly some yet incompletely explained bubble structures [18], and can be easily implemented in any geometry using COMSOL [22], for low frequency ultrasonics. It was shown in the latter references that our model, contrarily to linear acoustics and earlier cavitation models, correctly catches the strong wave attenuation near the emitter observable in presence of cavitation. As acoustic streaming is a matter of wave attenuation [6], it follows logically that a correct prediction of the latter is a pre-requisite for a viable evaluation of the former. Our model will be shown to compare reasonably well with the experiments reported in [20], and explains the persistence of cavitation even when the streaming jet is deflected.

2. Acoustic streaming models

The most popular model of acoustic streaming is attributed to Eckart [2], although Rayleigh [1], Westervelt [3] and Nyborg [4] contributed to the same result, and even found more general ones. As Eckart and Nyborg are names widely associated with streaming, we will refer to these results as Eckart–Nyborg's theory

E-mail address: louisnar@enstimac.fr

hereinafter. This model results from a regular perturbation procedure on compressible Navier–Stokes equations and exhibits the driving force for streaming as:

$$\mathbf{f} = -\nabla\left(\rho_{l_0}\overline{\mathbf{u}_1 \otimes \mathbf{u}_1}\right), \tag{1}$$

where $\mathbf{u}_1$ is the primary acoustic velocity field, ρ_{l_0} the liquid density at rest, overlined symbols denote averaged quantities over one acoustic period, and $\otimes$ is the dyadic product. The tensor in the divergence operator is the analog of the so-called "Reynolds stress tensor" in turbulence. In normal conditions (i.e. waves of moderate amplitude and no cavitation), $\mathbf{u}_1$ can be calculated from the equations of linear acoustics. Physically, the force density $\mathbf{f}$ represents an unbalance between the average (acoustic-induced) momentum entering and outgoing a given fluid volume. This unbalance must be compensated by a steady flow, which is precisely acoustic streaming.

The perturbation method followed by Eckart and Nyborg on mass and momentum conservation equations leads naturally to the following ones, governing the streaming velocity field:

$$0 = \nabla \cdot (\rho_{l_0}\mathbf{u}_m) + \nabla \cdot (\overline{\rho_1 \mathbf{u}_1}), \tag{2}$$

$$0 = \mathbf{f} - \nabla p_m + \mu_l \nabla^2 \mathbf{u}_m, \tag{3}$$

where ρ_1 is the density variation associated with the primary acoustic field, all quantities with subscript m denote the steady flow defining acoustic streaming, μ_l is the liquid dynamic viscosity, and the force density $\mathbf{f}$ is defined by Eq. (1).

It can be noted that Eq. (3) is nothing else that the momentum equation of a creeping flow (driven by force $\mathbf{f}$), that is the reduction of Navier–Stokes equation to Reynolds numbers $\ll 1$. Lighthill, following this line of reasoning, argued that despite Eq. (1) is the correct expression of the driving force, its use in Eq. (3) reduces the applicability of Eckart–Nyborg's theory to very low acoustic intensities, for which the streaming velocities are low enough to fulfill $\mathrm{Re} \ll 1$. Cavitation experiments involve Reynolds numbers of several thousands [14], and lie therefore clearly outside this range of applicability. As an numerical illustration, consider for example a 10 mm sonotrode in water. A Reynolds number of 1 would correspond to a streaming characteristic velocity of 0.1 mm s^{-1}, which is by far much lower than commonly observed.

Lighthill suggested therefore that, rather than from Eq. (3), the streaming velocity $\mathbf{u}_m$ should be calculated from the full steady Navier–Stokes equation (written here in conservative form):

$$\nabla\left(\rho_{l_0}\mathbf{u}_m \otimes \mathbf{u}_m\right) = \mathbf{f} - \nabla p_m + \mu_l \nabla^2 \mathbf{u}_m. \tag{4}$$

This equation was first derived by Zarembo [5] and defines what is generally termed as "Stuart streaming" [6,23], or "fast streaming" [24] as opposed to "slow streaming" which refers to Eckart–Nyborg's results.

The present model is based on the following hypothesis:

1. The first crucial assumption is to use magenta Stuart-Lighthill Eq. (4) rather than Eq. (3). Moreover, the acoustic streaming flows observed under cavitation are not only far from creeping flows, but are generally turbulent, as is clearly demonstrated in Refs. [8,14]. Thus, one should solve Eq. (4) for a turbulent flow. As is well-known, such flows presents small-scale eddies which are difficult, if not impossible, to solve directly by Navier–Stokes equations. Dedicated methods are therefore needed to seek turbulent solutions of Eq. (4).
2. On the other hand, the intensity of acoustic streaming is directly linked to the wave attenuation, as discussed in Ref. [6], [Section 4]. In this regard, it was shown in Ref. [25] that in presence of cavitation, the energy dissipated by the bubbles was the essential contribution to wave attenuation. This energy dissipation was calculated from numerically computed radial dynamics of inertial bubbles, allowing to simplify the model of Caflish et al. [26] into a nonlinear Helmholtz equation [21]. The resulting model was found to yield correct acoustic pressure levels in some typical configurations. More importantly, the strong wave attenuation was found to generate traveling waves [18], which are the only way to explain bubble strong ejection from the transducer [27]. The use of this realistic model of wave propagation is the second crucial point to the success of the present method.

Several theoretical predictions of acoustic streaming velocity fields in cavitating liquids have been proposed in the literature, either using Eckart–Nyborg Eq. (3) or Stuart-Lighthill Eq. (4). Most models pre-calculate the acoustic field in order to evaluate the driving force (1), generally by linear acoustics (possibly using a uniform attenuation coefficient as a free parameter) [28,29,10,11]. More complex but cavitation-unspecific acoustic models have also been tried [30]. Sajjadi and co-workers [31,32] derived simultaneously the acoustic and velocity fields from a time-dependent resolution of a two-phase model [33] describing the motion of a liquid containing vapor bubbles.[1] Kumar and co-workers [8,30] by-passed the computation of the acoustic field by using experimental LDA measurements of velocities and turbulence parameters as boundary conditions for the hydrodynamic problem. Trujillo & Knoerzer [23] proposed two original methods to compute the turbulent streaming jet without explicitly evaluating the acoustic field. The only input to their model is the input power, complemented by a single fitting parameter in each case. The methods follows closely Lighthill's derivation of the turbulent jet properties in the context of Stuart streaming, when either the driving force (1) can be considered as concentrated in one point, or a damped gaussian acoustic beam is considered. Surprisingly, these two simple and elegant methods show remarkable agreement with the experimental results of Kumar et al. [8].

The present model, even if it shares the use of Stuart-Lighthill Eq. (4) with some earlier models, differs from the latter in that our wave Eq. (5) accounts for the real energy disspation by an inertial bubble, rather than setting an empirical value to wave attenuation.

To conclude the discussion on acoustic streaming models, the derivation of Eq. (4) deserves a few comments. On the one hand, it requires a more subtle perturbation method than Eckart–Nyborg's theory, in order to avoid the natural disappearance of the inertial term in the left hand side [5,24]. On the other hand, there is no trivial justification of its validity within a cavitation model, which involves a two-phase flow. In other words, whether the driving force for streaming Eq. (1) is still valid with $\mathbf{u}_1$ calculated from our propagation model (which originates from Caflish model [26]) may be questioned. We will not enter more deeply in this discussion here, and it will be shown elsewhere that the set constituted by Caflish equations, Stuart-Lighthill Eq. (4 divergence-less field equation $\nabla \cdot \mathbf{u}_m = 0$ instead of Eq. (2), can be recovered by a perturbation method performed on the Van Wijngaarden equations [35].

[1] Singhal's model [33] is a classical hydrodynamic cavitation model, normally restricted to bubbly liquid containing only vapor bubbles, which allows a simple closure of the two-phase equations. The assumptions made in this model normally prohibit its use for inertial acoustic cavitation bubbles, in spite of its increasing popularity in the latter context. Its use should be restricted to the special case where the transducer tip is covered entirely by the gas/vapor phase for long time intervals [34].

3. Simulation methods

The problem solved corresponds to the experiments described in Refs [19,20] (Fig. 1). A rectangular duct $H = 35$ mm $\times$ $W = 40$ mm $\times$ $L = 140$ mm was fed with water flowing from left to right with an adjustable flow rate. The duct was equipped with a 20 kHz titanium horn on its bottom side at mid-length, emitting upwards in the duct. The horn section is a 22 mm $\times$ 25 mm truncated disk. The velocity field of the acoustic streaming superposed with the transverse forced flow was measured by PIV using a laser sheet illuminating the mid plane of the duct.

In order to obtain reasonably short calculations allowing parametric studies, the problem was simplified by considering a 2D geometry (Fig. 2), assuming infinite size in the z direction on Fig. 1. The results obtained hereinafter should therefore be considered as what would be measured in the xy mid-plane of the duct (containing the laser sheet).

The problem was then solved with COMSOL in two steps: the first one solves for the acoustic field and the second uses this result to calculate the force density (1) and solve Eq. (4) for the flow velocity.

For the interested reader, the main steps of the computations are summarized in Algorithm 1.

3.1. Acoustic field model

The model of acoustic waves propagation accounting for the presence of inertial cavitation is described in Refs. [21,22]. Considering only the harmonic part of the acoustic pressure field $p_1(\mathbf{r},t) = \Re(P_1(\mathbf{r})e^{i\omega t})$, the complex amplitude $P_1(\mathbf{r})$ is shown to approximately fulfill a nonlinear Helmholtz equation:

$$\nabla^2 P_1 + k^2(|P_1|)P_1 = 0, \tag{5}$$

where the complex squared wavenumber k^2 depends on the local pressure amplitude $|P_1|$, and is related to the energy dissipated by bubbles because of viscous friction [25,21] (see also Ref. [36] for a refinement of these results). The viscous dissipation function was pre-calculated using the model of bubble radial dynamics of Ref. [37] for $R_0 = 5$ µm air bubbles in water at ambient temperature, driven at 20 kHz.

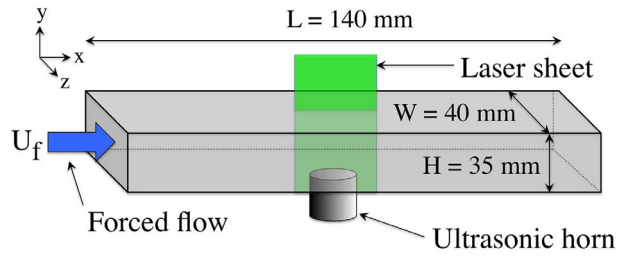

Fig. 1. Simulated experimental configuration [19,20]. The laser sheet lies in the xy plane. The transducer face lies in the xz plane and is flush with the internal face of the duct bottom wall. The forced flow enters the tube perpendicular to yz plane.

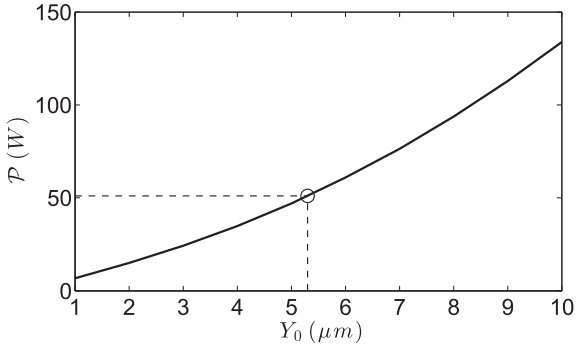

Fig. 3. Acoustic power transmitted to the liquid in function of the transducer displacement. The circle symbol indicates the transducer amplitude $Y_0 = 5.3$ µm for which the transmitted power is 51 W.

The inlet and outlet boundaries of the duct were assigned to the impedance of pure water. The transducer displacement Y_0 was imposed and all other boundaries were considered as perfectly hard.

The acoustic field was first calculated for a displacement of the transducer Y_0 ranging between 5 µm and 15 µm, and the resulting acoustic power $\mathcal{P}$ across the transducer was calculated for each Y_0. From the resulting curve (Fig. 3), the transducer displacement yielding the power reported in Ref. [20] ($\mathcal{P} = 51$ W) was calculated $Y_0 = 5.3$ µm and used in subsequent computations.

3.2. Hydrodynamics model

From the acoustic field computed in the above conditions, the volumetric force density (1) is evaluated and injected in Eq. (4), assuming furthermore incompressible flow $\nabla \cdot \mathbf{u}_m = 0$.

Since the flow is expected to be turbulent, direct Navier–Stokes equations cannot be solved directly. Instead, they are averaged and the randomly fluctuating part of the field is recast into a couple of additional continuous fields, supposed to represent the turbulence characteristics. Several choices are possible for these two fields but here, for simplicity, we chose the $k-\epsilon$ method which is computationally cheap and routinely used in engineering applications [38,39].

The hydrodynamics boundary conditions (Fig. 4) are set to imposed velocity U_f on inlet, default exit conditions at outlet, and turbulent wall functions on solid walls and transducer face [40]. The inlet velocity is varied in the range covered by experiments [20] through the corresponding Reynolds number

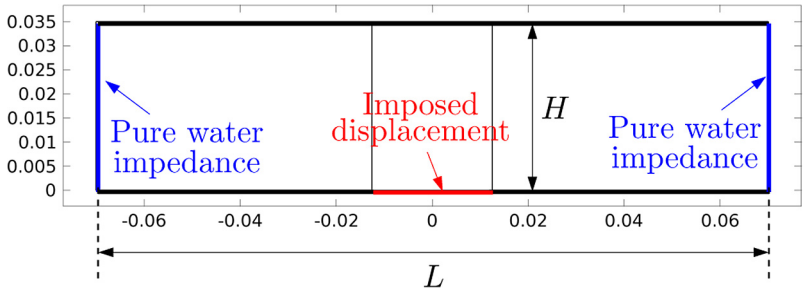

Fig. 2. Simulated 2D geometry and boundary conditions for the acoustic simulation. The vertical black thin lines materialize the transducer diameter.

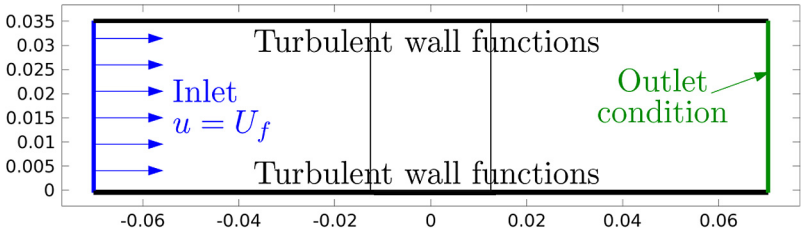

Fig. 4. (Color online) Hydrodynamic boundary conditions for computation of the turbulent flow.

$\mathrm{Re} = U_f D_h/\nu$ between 0 and 14000, where $D_h = 2\,WH/(W+H)$ is the equivalent hydraulic diameter [41] of the rectangular duct, and ν is the kinematic viscosity of the liquid.

Algorithm 1.: Main steps of the computation.

for $Y_0 \leftarrow 5$ µm **to** 15 µm **step** 1 µm **do**
  Compute acoustic pressure field P_1 ;
    (solving Eq. 5) ;
  Acoutic velocity field $\mathbf{U_1} \longleftarrow \dfrac{1}{\rho_l \omega^2}\boldsymbol{\nabla} P_1$;
  Acoustic power $\mathcal{P} \longleftarrow \displaystyle\iint_{S_{\text{transducer}}} \frac{1}{2}\Re(P_1^* \mathbf{U_1}).\mathbf{n}\, dS$
Select Y_0 for which $\mathcal{P} = 51$ W ;
Re-compute P_1 and $\mathbf{U_1}$ for this value ;
Compute $(\overline{\mathbf{u_1} \otimes \mathbf{u_1}})_{ij} = \frac{1}{2}\Re\left(U_{1i}U_{1j}^*\right)$;
Compute force $f_i = -\dfrac{\partial\left(\rho_{l_0}(\overline{\mathbf{u_1} \otimes \mathbf{u_1}})_{ij}\right)}{\partial x_j}$;
for $Re \leftarrow 0$ **to** 13000 **step** 1000 **do**
  Inlet velocity $U_f \longleftarrow \mathrm{Re}\dfrac{\nu}{D_h}$;
  Compute streaming velocity field $\mathbf{u}_\mathrm{m}$;
    (solving Eq. 4 by $k-\epsilon$) ;

4. Results

4.1. Acoustic field

The acoustic field obtained for $Y_0 = 5.3$ µm is presented on Fig. 5. Two regions subject to large acoustic pressures appear. One is located just above the transducer and correspond to damped traveling waves, similarly to what happens in cone bubble structures [18]. The other is located near the solid wall facing the transducer and corresponds to the antinode of a standing wave. The Blake threshold is materialized by a (blue online) thick solid line, and all the enclosed regions may be assumed to be the locus of bubble nucleation and subsequent inertial oscillations.

Since computation of acoustic streaming is generally associated to the choice of a wave attenuation coefficient $\alpha = -\Im(k)$, we extracted the latter from our computation. The evolution of α along the vertical symmetry axis at $x = 0$, and along the vertical line materializing the transducer diameter $x = 1.25cm$, is presented as supplementary material (Fig. S1).

4.2. Velocity field

Fig. 6 displays the velocity fields obtained for increasing Reynolds numbers of the transverse forced flow. The color level represents the velocity amplitude.

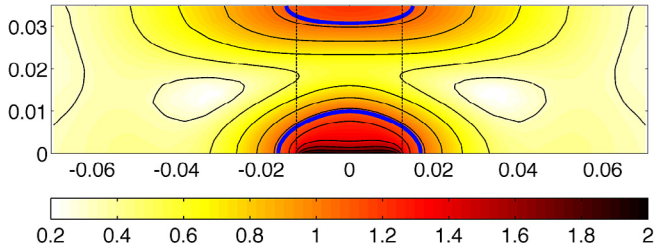

Fig. 5. (Color online) Acoustic field calculated from Eq. (5) for a transducer displacement amplitude $Y_0 = 5.3$ µm. The color levels represent the acoustic pressure amplitude $|P_1|$ non-dimensionalized by ambient pressure p_0. The thin solid lines are the contour curve corresponding to the color bar graduations and have been included for better readability. The thick solid line (blue online) is the Blake threshold locus. The vertical dashed lines materializes the transducer diameter.

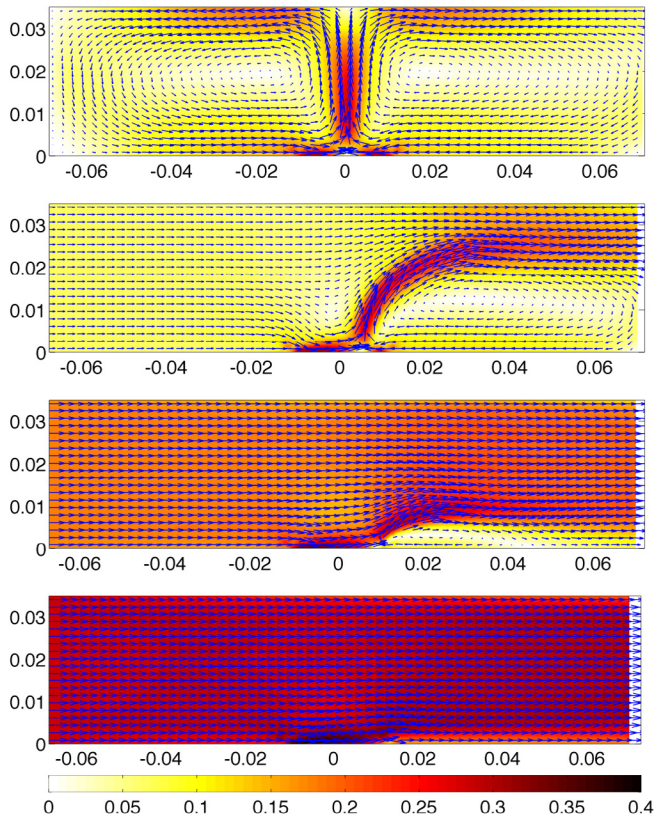

Fig. 6. (Color online) Velocity field for a Reynolds number of the forced flow Re = 0, 3000, 8000, 13000 (from top to bottom). The arrow have been normalized for better readability and their length do not scale with the velocity amplitude. The latter is represented by the color level in ms^{-1}.

In absence of forced flow (top graph), the acoustic streaming jet flows upwards with two lateral vortices. The shape of the jet as well as the order of magnitude of the jet velocity (typically

0.3 ms^{-1}) agree remarkably well with the experimental results of Refs. [19,20] [2]

In presence of a transverse forced flow in the duct (three bottom graphs on Fig. 6), the jet is increasingly deflected as the inlet velocity increases. Here again, the agreement with experimental results is remarkable. A closer examination shows however that for a given Reynolds of the transverse flow, the model slightly overestimates the jet deflection. This suggests that our estimation of the streaming velocity, and probably of the force density Eq. (1), are slightly underestimated.

4.3. Bubble paths

In our earlier works [18,22], where the liquid was assumed motionless, it was suggested that the paths followed by the bubbles could be equated to the streamlines of the primary Bjerknes force field, which can be readily calculated once the amplitude and phase of the acoustic field are known [42–44]. In the present work, owing to acoustic streaming and to the transverse flow, the liquid has a steady motion. The bubbles therefore suffer an additional steady drag force, whose effect on their motion should be quantified.

The general equation of motion of a bubble in the combined velocity field $\mathbf{u}_1 + \mathbf{u}_m$ would read [45–47], neglecting the bubble inertia, weight and buoyancy:

$$0 = \frac{1}{2}\rho_{l_0}\frac{d[V(\mathbf{u}_m + \mathbf{u}_1 - \mathbf{v})]}{dt} + 12\pi R\mu_l(\mathbf{u}_m + \mathbf{u}_1 - \mathbf{v}) - V\nabla(p_1 + p_m), \tag{6}$$

where $\mathbf{v}$ is the instantaneous velocity of the bubble, and V, R its instantaneous volume and radius, respectively. The first RHS term in Eq. (6) is the added-mass force [45], the second is the viscous force [48] and the third is the generalized buoyancy force, which, once averaged over one acoustic cycle, yields the well-known primary Bjerknes force. For simplicity we disregard the secondary Bjerknes force here.

We emphasize that in Eq. (6), $R, V, \mathbf{u}_1, \mathbf{v}$ and p_1 are all periodic functions of time. Because of that, time-average of their product do not necessarily cancel. Thus, even in absence of steady flow, averaging correctly Eq. (6) to get $\mathbf{v}$ is somewhat technical and has been the matter of several studies (in absence of steady liquid motion) [49–51]. As a consequence, calculating the velocity of a bubble is a difficult matter, reinforced by the fact that the radial and translational motion are in fact coupled [52,53]. As we are concerned here only with orders of magnitude, we will assume that Eq. (6) can be simply averaged into:

$$12\pi\langle R\rangle\mu_l(\langle\mathbf{v}\rangle_\infty - \mathbf{u}_m) = \langle -V\nabla p_1\rangle, \tag{7}$$

where $\langle\mathbf{v}\rangle_\infty$ is the terminal velocity of the bubble, $\langle R\rangle$ is the bubble radius averaged over one period, and the averaged quantity in the right-hand side is the classical primary Bjerknes force $\mathbf{F_B}$ [42,44]. Both quantities $\langle R\rangle$ and $\mathbf{F_B}$ are computed from separate bubble dynamics simulations over a given range of acoustic pressures [18, Section 2.2]. Eq. (7) finally yields the bubble terminal velocity:

$$\langle\mathbf{v}\rangle_\infty = \mathbf{u}_m + \frac{\mathbf{F_B}}{12\pi\langle R\rangle\mu_l}. \tag{8}$$

The physical meaning of this equation can be readily understood by considering two extreme cases: where the Bjerknes force is weak, the bubble will follow the steady flow ($\langle\mathbf{v}\rangle_\infty = \mathbf{u}_m$). On the contrary, for large values of the Bjerknes force, the bubble will be mainly driven by the latter, irrespective of the liquid flow $\mathbf{u}_m$.

[2] For brevity, we do not reproduce the cited experimental results here. The reader is referred to Ref. [20, Fig. 3].

This competition is illustrated on Fig. 7 which shows the streamlines of the flow $\mathbf{u}_m$ (forced + acoustic streaming), and the bubble paths calculated from Eq. (8), as the Reynolds of the transverse flow is increased. The conditions are the same as in Fig. 6. Bubbles are launched from a series of arbitrary points inside regions where the acoustic pressure exceeds the Blake threshold (see Ref. [18] for details).

Some bubble paths start from the transducer and converge towards a hemispherical cap, which also attracts bubbles nucleated above. Such structures are commonly found in experimental arrangements where the transducer area is at the same level as a surrounding solid wall [54], and share some similarities with cone bubble structures. It is clearly seen that the bubble paths do not necessarily coincide with the liquid streamlines. A similar observation can be found in Ref. [14]. Their slight deflection by the stream is however visible, especially near the Blake threshold locus.

A similar important feature caught by our model is the presence of cavitation bubbles near the wall facing the transducer, resulting from a pressure antinode in this zone. Since Bjerknes forces are large there, the bubbles are attracted by the wall and form a streamer, even for strong liquid flow perpendicular to the wave propagation. Thus, contrarily to what the velocity fields of Fig. 6 or [20], [Fig. 3] might intuitively suggest, bubbles always remain close to the wall facing the transducer. This feature has been indeed observed experimentally in this setup, and electrochemical measurements confirmed a cavitational activity on the wall facing the transducer even for strong transverse flow [19,20]. This allows an efficient ultrasonic cleaning of this surface (for example a boat hull) even in presence of a perpendicular flow whose function is to suck the dirt removed [55].

5. Models yielding unrealistic predictions

As mentioned in Section 2, the two key features of our model are a realistic prediction of the acoustic field, and solving the full equation of fluid motion for a turbulent flow. To reinforce this assertion, it is instructive to examine how do the above predictions evolve when one of these assumptions is relaxed.

5.1. Linear acoustics

Instead of the model presented in Ref. [21], we use the equations of linear acoustics, keeping the same displacement amplitude of the transducer as above. The resulting acoustic pressure is shown on Fig. 8. It is seen that the acoustic pressure reaches unrealistic huge values. This was already demonstrated in Ref. [21], and is the consequence of disregarding dissipation by cavitation bubbles. Similar results were obtained in Ref. [56], with a different approach (see their Fig. 6 and the discussion in appendix of Ref. [22]).

The corresponding velocity field in absence of forced flow is presented on Fig. 9. Despite the range of velocities is in agreement with experiments, their spatial distribution is wrongly predicted. In particular the velocities inside the jet are clearly underestimated.

5.2. Eckart–Nyborg's model

Finally, we turn back to our nonlinear propagation model Eq. (5), but evaluate the streaming velocity field by Eckart–Nyborg's Eq. (3) instead of the Stuart-Lighthill Eq. (4). As mentioned above, this reverts to neglect the inertial term in Navier–Stokes equation and assume that the flow is in the creeping regime, that is $\mathrm{Re} \ll 1$.

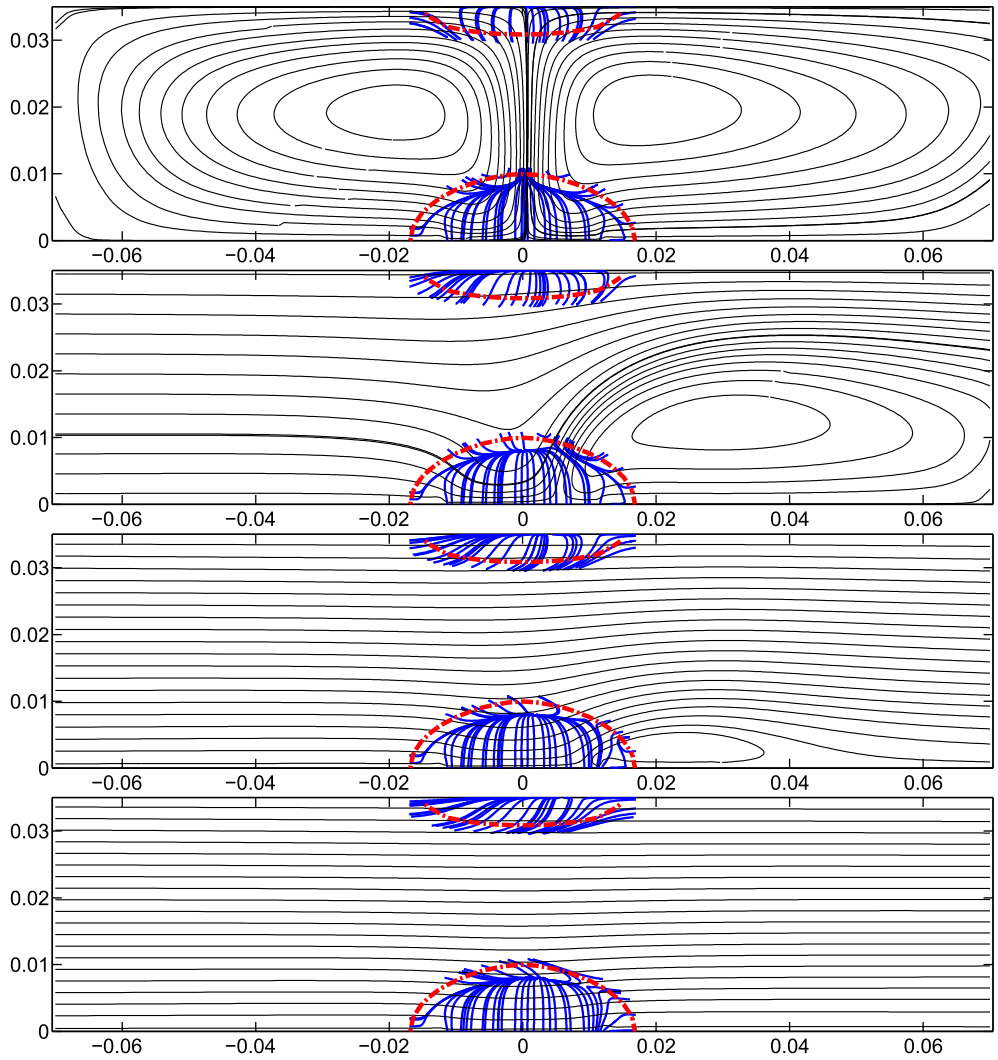

Fig. 7. (Color online) From top to bottom Re = 0, 3000, 8000, 13000. Thin lines (black online): streamlines of the flow. Thick lines attached to top and bottom walls (blue online): predicted path of the bubbles, under the common action of the flow and Bjerknes forces. As in Refs. [18,22], the bubbles are launched arbitrarily from any point where the acoustic pressure exceeds 0.95 × the Blake threshold. The latter is materialized by thick dashed lines (red online). (For interpretation of the references to colour in this figure legend, the reader is referred to the web version of this article.)

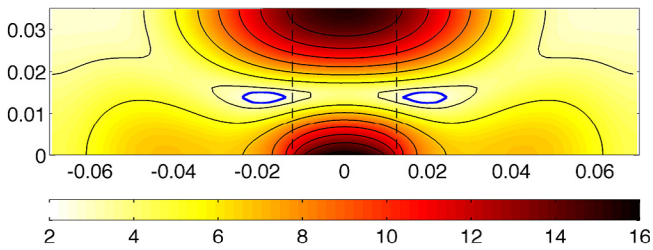

Fig. 8. (Color online) Acoustic field calculated from linear acoustics, for a transducer displacement amplitude $Y_0 = 5.3$ μm. The color levels represent the acoustic pressure amplitude $|P_1|$ non-dimensionalized by ambient pressure p_0. The thin solid lines are the contour curve corresponding to the color bar graduations and have been included for better readability. The thick solid line (blue online) is the Blake threshold locus. The vertical dashed lines materializes the transducer diameter. (For interpretation of the references to colour in this figure legend, the reader is referred to the web version of this article.)

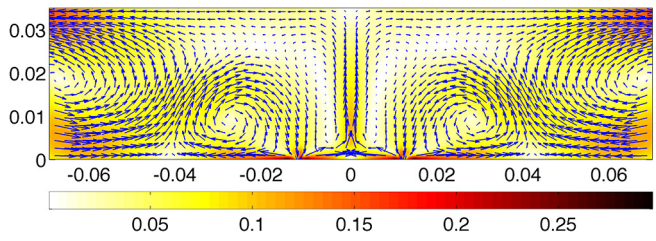

Fig. 9. (Color online) Velocity field in absence of forced flow with acoustic field calculated from linear acoustics.

The result is displayed on Fig. 10 and shows a large discrepancy with the experimental one, not only in shape, but also in magnitude. Eckart–Nyborg's theory overestimate velocities by one order of magnitude (with a maximum around 10 ms^{-1}).

In fact, this failure could be easily expected, since the presence of a jet with marked boundaries, as commonly observed in many cavitation experiments [12,14,20], is contradictory with the definition of a creeping flow. Indeed, in the latter, momentum transport is governed by diffusion only, which would smooth out any sharp velocity gradient. This is a well-known result covered by any textbook of Fluid Mechanics, and a nice visual illustration can be found in the film of US National Committee for Fluid Mechanics Films [57], Chap. "*Low Reynolds number flows*".

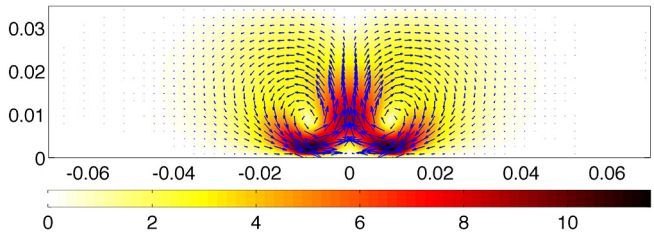

Fig. 10. (Color online) Velocity field in absence of forced flow, following Eckart–Nyborg's theory. The color level represents the velocity in ms^{-1}

6. Summary and conclusions

1. We have shown that a reasonably good quantitative prediction of acoustic streaming in presence of cavitation can be obtained by seeking the turbulent solution of the incompressible Navier–Stokes equations, driven by the volumetric force Eq. (1), provided the acoustic field injected in the latter is calculated by Louisnard's model [21].
2. The model catches the fact that bubbles are not necessarily dragged by the steady flow, and that they follow the primary Bjerknes force field in regions of high acoustic fields, as if the liquid were at rest. This explains why cavitational activity is still observed in front of the transducer in experiments of Refs. [19,20]
3. Linear acoustics on one hand, and Eckart–Nyborg's theory on the other hand, have been shown to yield unrealistic results. As this model implicitly assumes a creeping flow, it is anyway unable to represent turbulent jets classically observed in cavitation experiments.

These results can be refined in several ways, first by performing full 3D simulations. Second, the use of $k-\epsilon$ method to solve for the turbulent flow can be easily replaced by more elaborate turbulent numerical methods [30]. Then, the simulation of other experimental configurations is under consideration.

Additionally, it will be shown elsewhere how the equations used in the present work (Caflish model and streaming equations) can be derived jointly from van Wijngaarden equations [35]. Finally, Louisnard's model of wave propagation [21] can still be enhanced, especially to account for poly-disperse bubble sizes and bubble densities varying with the local acoustic pressure. A more rigorous calculation of bubble paths is also under consideration.

Acknowledgement

The author would like to thank Magali Barthes and Jean-Yves Hihn from University of Besançon for fruitful discussions and clarifications on their experimental setup.

Appendix A. Supplementary data

Supplementary data associated with this article can be found, in the online version, at http://dx.doi.org/10.1016/j.ultsonch.2016.09.013.

References

[1] L. Rayleigh, Theory of sound, Dover Publications, 1896, Ch. 352.
[2] C. Eckart, Phys. Rev. 73 (1) (1948) 68.
[3] P.J.P.J. Westervelt, J. Acoust. Soc. Am. 23 (3) (1951) 312–315.
[4] W.L. Nyborg, J. Acoust. Soc. Am. 25 (1) (1953) 68–75.
[5] L.K. Zarembo, in: L.D. Rozenberg (Ed.), High-Intensity Ultrasonic Fields, Plenum Press, 1971, pp. 135–199.
[6] J. Lighthill, J. Sound Vib. 61 (3) (1978) 391–418.
[7] N. Gondrexon, V. Renaudin, C. Petrier, M. Clement, P. Boldo, Y. Gonthier, A. Bernis, Ultrason. Sonochem. 5 (1) (1998) 1–6.
[8] A. Kumar, T. Kumaresan, A.B. Pandit, J.B. Joshi, Chem. Eng. Sci. 61 (22) (2006) 7410–7420.
[9] N.A. Tsochatzidis, P. Guiraud, A.M. Wilhelm, H. Delmas, Chem. Eng. Sci. 56 (5) (2001) 1831–1840.
[10] O. Dahlem, J. Reisse, V. Halloin, Chem. Eng. Sci. 54 (13) (1999) 2829–2838.
[11] M. Chouvellon, A. Largillier, T. Fournel, P. Boldo, Y. Gonthier, Ultrason. Sonochem. 7 (4) (2000) 207–211.
[12] A. Mandroyan, M.L. Doche, J.Y. Hihn, R. Viennet, Y. Bailly, L. Simonin, Ultrason. Sonochem. 16 (1) (2009) 97–104.
[13] J.Y. Hihn, M.L. Doche, A. Mandroyan, L. Hallez, B. Pollet, Ultrason. Sonochem. 18 (4) (2011) 881–887.
[14] T. Nowak, C. Cairós, E. Batyrshin, R. Mettin, Recent developments in nonlinear acoustics: 20th International Symposium on Nonlinear Acoustics including the 2nd International Sonic Boom Forum, vol. 1685, AIP Publishing, 2015, p. 020002.
[15] A. Moussatov, C. Granger, B. Dubus, Ultrason. Sonochem. 10 (2003) 191–195.
[16] C. Campos-Pozuelo, C. Granger, C. Vanhille, A. Moussatov, B. Dubus, Ultrason. Sonochem. 12 (2005) 79–84.
[17] B. Dubus, C. Vanhille, C. Campos-Pozuelo, C. Granger, Ultrason. Sonochem. 17 (2010) 810–818.
[18] O. Louisnard, Ultrason. Sonochem. 19 (2012) 66–76.
[19] G. Mazue, R. Viennet, J.Y. Hihn, D. Bonnet, M. Barthes, Y. Bailly, I. Albaïna, Récents Progrès en Génie des Procédés 104 (sfgp2013120323) (2013) 1–8.
[20] M. Barthès, G. Mazue, D. Bonnet, R. Viennet, J.Y. Hihn, Y. Bailly, Ultrasonics 59 (2015) 72–78.
[21] O. Louisnard, Ultrason. Sonochem. 19 (2012) 56–65.
[22] O. Louisnard, C. Cogné, S. Labouret, W. Montes-Quiroz, R. Peczalski, F. Baillon, F. Espitalier, Ultrason. Sonochem. 26 (2015) 186–192.
[23] F.J. Trujillo, K. Knoerzer, Ultrason. Sonochem. 18 (6) (2011) 1263–1273.
[24] J. Friend, L.Y. Yeo, Rev. Mod. Phys. 83 (2) (2011) 647.
[25] O. Louisnard, Phys. Procedia 3 (1) (2010) 735–742, international Congress on Ultrasonics, Santiago de Chile, January 2009.
[26] R.E. Caflish, M.J. Miksis, G.C. Papanicolaou, L. Ting, J. Fluid Mech. 153 (1985) 259–273.
[27] P. Koch, R. Mettin, W. Lauterborn, in: D. Cassereau (Ed.), Proceedings CFA/DAGA'04 Strasbourg, Oldenburg, DEGA, 2004, pp. 919–920.
[28] Z. Xu, K. Yasuda, S. Koda, Ultrason. Sonochem. 20 (1) (2013) 452–459.
[29] Q. Jiao, X. Tan, J. Zhu, Ultrason. Sonochem. 21 (2) (2014) 535–541.
[30] T. Kumaresan, A. Kumar, A.B. Pandit, J.B. Joshi, Ind. Eng. Chem. Res. 46 (10) (2007) 2936–2950.
[31] B. Sajjadi, A.A.A. Raman, S. Ibrahim, Ultrason. Sonochem. 27 (2015) 359–373.
[32] B. Sajjadi, A.A.A. Raman, S. Ibrahim, Ultrason. Sonochem. 24 (2015) 193–203.
[33] A.K. Singhal, M.M. Athavale, H. Li, Y. Jiang, J. Fluids Eng. 124 (3) (2002) 617–624.
[34] A. Žnidarčič, R. Mettin, M. Dular, Ultrason. Sonochem. 22 (2015) 482–492.
[35] L. van Wijngaarden, J. Fluid Mech. 33 (3) (1968) 465–474.
[36] R. Jamshidi, G. Brenner, Ultrasonics 53 (4) (2013) 842–848.
[37] R. Toegel, B. Gompf, R. Pecha, D. Lohse, Phys. Rev. Lett. 85 (15) (2000) 3165–3168.
[38] B.E. Launder, D.B. Spalding, Comput. Methods Appl. Mech. Eng. 3 (2) (1974) 269–289.
[39] D.C. Wilcox, Turbulence modeling for CFD, DCW industries La Canada, CA, 1998.
[40] COMSOL Multiphysics 4.2, in: CFD Module User's Guide, COMSOL AB, Stockholm, Sweden, 2011.
[41] F.M. White, Fluid mechanics, Mc Graw-Hill, 1994.
[42] I. Akhatov, R. Mettin, C.D. Ohl, U. Parlitz, W. Lauterborn, Phys. Rev. E 55 (3) (1997) 3747–3750.
[43] P. Koch, D. Krefting, T. Tervo, R. Mettin, W. Lauterborn, Proc. ICA 2004, Kyoto (Japan), vol. Fr3.A.2, 2004, pp. V3571–V3572.
[44] R. Mettin, in: A.A. Doinikov (Ed.), Bubble and particle dynamics in acoustic fields: modern trends and applications, Research Signpost, Kerala (India), 2005, pp. 1–36.
[45] J. Magnaudet, I. Eames, Ann. Rev. Fluid Mech. 32 (2000) 659–708.
[46] U. Parlitz, R. Mettin, S. Luther, I. Akhatov, M. Voss, W. Lauterborn, Philos. Trans. R. Soc. London A 357 (1999) 313–334.
[47] R. Mettin, in: T. Kurz, U. Parlitz, U. Kaatze (Eds.), Oscillations, Waves and Interactions, Universitätsverlag Göttingen, 2007, pp. 171–198.
[48] J. Magnaudet, D. Legendre, Phys. Fluids 10 (1998) 550–554.
[49] A.J. Reddy, A.J. Szeri, J. Acoust. Soc. Am. 112 (2002) 1346–1352.
[50] D. Krefting, J.O. Toilliez, A.J. Szeri, R. Mettin, W. Lauterborn, J. Acoust. Soc. Am. 120 (2) (2006) 670–675.
[51] J.O. Toilliez, A.J. Szeri, J. Acoust. Soc. Am. 123 (4) (2008) 1916–1930.
[52] A.A. Doinikov, Recent Res. Devel. Acoustics 2 (2005) 13–38.
[53] R. Mettin, A.A. Doinikov, Appl. Acoust. 70 (2009) 1330–1339.
[54] V. Salinas, Y. Vargas, O. Louisnard, L. Gaete, Ultrason. Sonochem. 22 (2015) 227–234.
[55] G. Mazue, R. Viennet, J.Y. Hihn, L. Carpentier, P. Devidal, I. Albaïna, Ultrason. Sonochem. 18 (4) (2011) 895–900.
[56] K. Yasui, Y. Iida, T. Tuziuti, T. Kozuka, A. Towata, Phys. Rev. E 77 (1) (2008) 016609.
[57] N.C. for Fluid Mechanics Films, Illustrated experiments in fluid mechanics: the NCFMF book of film notes, MIT Press, 1972. http://web.mit.edu/hml/ncfmf.html.